Influence of sediment settling velocity on mechanistic soil erosion modeling

Tromp-van Meerveld, H J ; Parlange, Jean-Yves ; Barry, D A ; Tromp, M F ; Sander, Graham C ; Walter, M Todd ; Parlange, Marc B

Abstract: We report on a series of soil erosion experiments performed on the 2-m × 6-m EPFL erosion flume. Total sediment concentrations and the concentrations of seven size fractions (<2, 2–20, 20–50, 50–100, 100–315, 315–1000, and >1000 m) were measured during 14 high-intensity (47.5–52.5 mm/h) rainfall experiments on three different slopes (2.2–12.4%). The short-time and long-time analytical solutions for the Hairsine-Rose erosion model were rewritten to account for infiltration. The newly collected data were used to test the model under conditions that had not been explored before (steeper slopes, infiltration, more realistic soil composition). The analytical solutions could predict the observed total sediment concentration well. However, the observed sediment concentrations for the individual size classes could be predicted only when adjusted settling velocities were used. The adjusted settling velocities were estimated through manual optimization. The optimized settling velocities for the smallest and midsize particles (<100 m) were larger than calculated from Stokes' law or measured in a 0.47-m tube, while the optimized settling velocities for the largest particles (>315 m) were smaller than measured. The effective settling velocities could also be calculated from the calculated amount of material in the shield of each size class at the end of the experiments. This calculated settling velocity distribution agreed very well with the optimized settling velocities. This study moves the Hairsine-Rose model another step closer to an operational soil erosion model for field applications.

DOI: https://doi.org/10.1029/2007WR006361

Influence of sediment settling velocity on mechanistic soil erosion modeling

H. J. Tromp-van Meerveld,[1,2] J.-Y. Parlange,[3] D. A. Barry,[2] M. F. Tromp,[2] G. C. Sander,[4] M. T. Walter,[3] and M. B. Parlange[2]

Received 19 July 2007; revised 24 January 2008; accepted 25 February 2008; published 3 June 2008.

[1] We report on a series of soil erosion experiments performed on the 2-m × 6-m EPFL erosion flume. Total sediment concentrations and the concentrations of seven size fractions (<2, 2–20, 20–50, 50–100, 100–315, 315–1000, and >1000 μm) were measured during 14 high-intensity (47.5–52.5 mm/h) rainfall experiments on three different slopes (2.2–12.4%). The short-time and long-time analytical solutions for the Hairsine-Rose erosion model were rewritten to account for infiltration. The newly collected data were used to test the model under conditions that had not been explored before (steeper slopes, infiltration, more realistic soil composition). The analytical solutions could predict the observed total sediment concentration well. However, the observed sediment concentrations for the individual size classes could be predicted only when adjusted settling velocities were used. The adjusted settling velocities were estimated through manual optimization. The optimized settling velocities for the smallest and midsize particles (<100 μm) were larger than calculated from Stokes' law or measured in a 0.47-m tube, while the optimized settling velocities for the largest particles (>315 μm) were smaller than measured. The effective settling velocities could also be calculated from the calculated amount of material in the shield of each size class at the end of the experiments. This calculated settling velocity distribution agreed very well with the optimized settling velocities. This study moves the Hairsine-Rose model another step closer to an operational soil erosion model for field applications.

Citation: Tromp-van Meerveld, H. J., J.-Y. Parlange, D. A. Barry, M. F. Tromp, G. C. Sander, M. T. Walter, and M. B. Parlange (2008), Influence of sediment settling velocity on mechanistic soil erosion modeling, *Water Resour. Res.*, *44*, W06401, doi:10.1029/2007WR006361.

1. Introduction

[2] Many studies have shown that interrill soil erosion is a size-selective process [*Swanson et al.*, 1965; *Young and Onstad*, 1976; *Gabriels and Moldenhauer*, 1978; *Mitchell et al.*, 1980; *Miller and Baharuddin*, 1987; *Proffitt et al.*, 1991; *Sutherland et al.*, 1996; *Slattery and Burt*, 1997; *Wan and El-Swaify*, 1998; *Basic et al.*, 2002; *Leguédois and Bissonnais*, 2004; *Malam Issa et al.*, 2006; *Asadi et al.*, 2007]. Most of these studies reported that the eroded soil is enriched in clay and silt-sized particles relative to the original soil. A better understanding of the dynamics of the suspended sediment concentrations of individual particles, as well as the total sediment concentration, will improve understanding of erosion and sedimentation processes. Because chemicals (e.g., phosphorus) are preferentially sorbed to the small (i.e., clay) particles, it can also provide the basis for improved understanding of the transfer of nonpoint source nutrients and pollutants to waterways and the ability to better model these fluxes.

[3] The two main processes in rainfall-driven interrill soil erosion are the detachment of soil particles due to the impact of raindrops and transport of particles, principally by overland flow. After soil particles become detached and suspended, they fall back toward the soil surface due to their immersed weight. The large particles return to the soil surface quickly while the small particles, which have smaller settling velocities, are carried significant distances in the direction of the surface water flow before falling back to the soil surface. Therefore, at the beginning of an erosion event, most of the contribution to the total suspended sediment comes from the finer particles. However, with increasing time most of the finer material has been removed and the contribution of larger particles to the total sediment concentration increases [*Proffitt et al.*, 1991].

[4] *Hairsine and Rose* [1991] and *Rose et al.* [1994] developed a multiple particle size physical soil erosion model for rain-impacted flows in the absence of entrainment by overland flow. Hereinafter we refer to this multiple particle size model as the Hairsine-Rose model. In contrast with other soil erosion models that often lump or average oversize classes, the Hairsine-Rose model considers the

[1]Department of Geography, Simon Fraser University, Burnaby, British Columbia, Canada.
[2]Institute of Environmental Science and Technology, School of Architecture, Civil and Environmental Engineering, Ecole Polytechnique Fédérale de Lausanne, Lausanne, Switzerland.
[3]Department of Biological and Environmental Engineering, Cornell University, Ithaca, New York, USA.
[4]Department of Civil and Building Engineering, Loughborough University, Loughborough, UK.

0043-1397/08/2007WR006361

contributions of the individual size classes to the total suspended sediment concentration. *Sander et al.* [1996] assumed spatial independence and obtained a simplified numerical solution for the Hairsine-Rose model. This numerical solution agreed well with the experimental data for the total sediment concentration from *Proffitt et al.* [1991]. *Parlange et al.* [1999] then used a time decoupling to derive simple analytical solutions. Their short-time solution considered processes associated with the rainfall impact while the longer time solution described the behavior controlled by advection. They showed that their solutions were comparable to the numerical solutions of *Sander et al.* [1996]. Being analytical, they more readily aid in our understanding of soil erosion mechanisms. The solutions of *Parlange et al.* [1999] were developed for the case where there is no infiltration and precipitation equals runoff. Here we rewrite their solutions to account for infiltration. In addition, we introduce two more simplifications to the long-time solution.

[5] The Hairsine-Rose model for rainfall-induced soil erosion has been tested with a limited amount of experimental data. These were mainly (1) the *Proffitt et al.* [1991] flume experiments under very low slopes on a clay and a sandy clay loam soil, (2) the small-scale horizontal experiments of *Heilig et al.* [2001a, 2001b] on an artificial soil consisting of 90% fine sand (180–212 μm) and 10% clay, and (3) the small-scale horizontal experiments of *Gao et al.* [2003] on a clay soil. The model validation for these experiments was reasonably successful. It is thus appropriate to extend the model validation to different circumstances. Here we consider more extreme slopes with infiltration and different soil compositions. As indicated above, the experimental results are analyzed using the *Parlange et al.* [1999] analytical solutions for the Hairsine-Rose model. In doing so, we are in a position to extend the analyses of *Sander et al.* [1996] and *Parlange et al.* [1999], and investigate how well the model represents the observed concentrations of the individual size fractions. Another issue stemming from this validation exercise is that of parameter identifiability.

2. Methods

2.1. Experimental Setup

2.1.1. Erosion Flume

[6] The erosion experiments were done at the EPFL erosion flume. The flume and sprinkling system are described by *Viani* [1986] and *Baril* [1991]. Here we describe the major components of the flume. The 6-m-long × 2-m-wide planar flume is equipped with a slope adjustment mechanism. The flume was filled with 0.32 m of a loam soil from an agricultural field near Sullens (Vaud), Switzerland, sitting on top of 0.10 m of coarse gravel to allow for vertical drainage. The relatively deep soils in combination with the drainage openings at the bottom and downslope end of the flume allowed us to do erosion experiments on unsaturated soils. Most other erosion experiments have been done on saturated soils or on very thin soils that likely became saturated during the experiment.

2.1.2. Water Application

[7] Water was applied to the flume from 10 Veejet 80150 nozzles (see Figure 1, number 5) located on two oscillating bars at 3 m above the soil surface (Figure 1, number 8) using water from nearby Lake Geneva. Collection troughs were located below the nozzles at both ends of each sweep (Figure 1, number 6) to control the amount of water applied. Water collected in these collection troughs flowed to the storm drain (Figure 1, number 7). The intensity of the precipitation could be adjusted by changing the interval of each sweep. The median size of the rainfall drops, measured using the flour method during previous experiments with the same nozzles, was ~2.2 mm [*Viani*, 1986]. The kinetic energy of these drops was ~24 J/m^2 per millimeter of precipitation [*Viani*, 1986].

[8] The spatial distribution of the rainfall was measured using 192 rainfall gauges, each with a 0.10-m-diameter orifice. The pressure at each nozzle was adjusted such that the spatial distribution of the applied rainfall was near uniform, with a uniformity coefficient [*Christiansen*, 1942] of 0.86 (independent of the rainfall intensity). We used these rainfall measurements also to determine the relation between the sprinkling interval and the average depth of water applied (r^2 = 0.998).

2.1.3. Water and Sediment Collection

[9] There were eight openings in the bottom of the flume to allow for vertical drainage. There were also two openings at the downslope end of the flume; one at 0.40 m below the soil surface draining the gravel and one at 0.21 m below the soil surface capturing subsurface flow through the soil (Figure 1, number 3). The openings were connected to hoses, which emptied into 0.2-m^3 buckets with stilling wells. The water level in the stilling wells was measured every 10 s with capacitance water level probes (Odyssey, Christchurch, New Zealand, http://www.odysseydatarecording.com). Vertical and lateral drainage rates were calculated from the measured water level rise in these collection buckets and the measured relation between water level and the volume of water in each bucket.

[10] Overland flow was collected at the downslope end of the flume in a large funnel under the overland flow collection trough (Figure 1, number 2). The large funnel led to another funnel and ultimately to a 0.2-m^3 bucket with a stilling well, similar to those used to capture the vertical and lateral drainage. When the overland flow bucket was full, the bucket was exchanged with a similar 0.2-m^3 bucket with a stilling well. The exchange of the overland flow buckets took ~1 min and thus resulted in an ~1-min data gap for the overland flow rate.

[11] Samples of the overland flow water and the sediments in it were collected manually in 0.5- and 1.0-L bottles under the funnel below the overland flow trough at the downslope end of the flume. The time between consecutive samples was <30 s at the beginning of the experiments and up to 15 min at the end of the experiments. We measured the time it took to fill the sample bottles and used this to cross-check the overland flow rate calculated from the water level rise in the bucket with the stilling well. The sediment in the sample bottles was allowed to settle for at least a week or until the water was clear. We then drained part of the water in the sample bottles and placed the bottles in an oven at 53°C to evaporate the remainder of the water. The oven-dried samples were weighed to obtain the amount and concentration of sediment in each sample. The size class distribution was determined for a subset of the collected

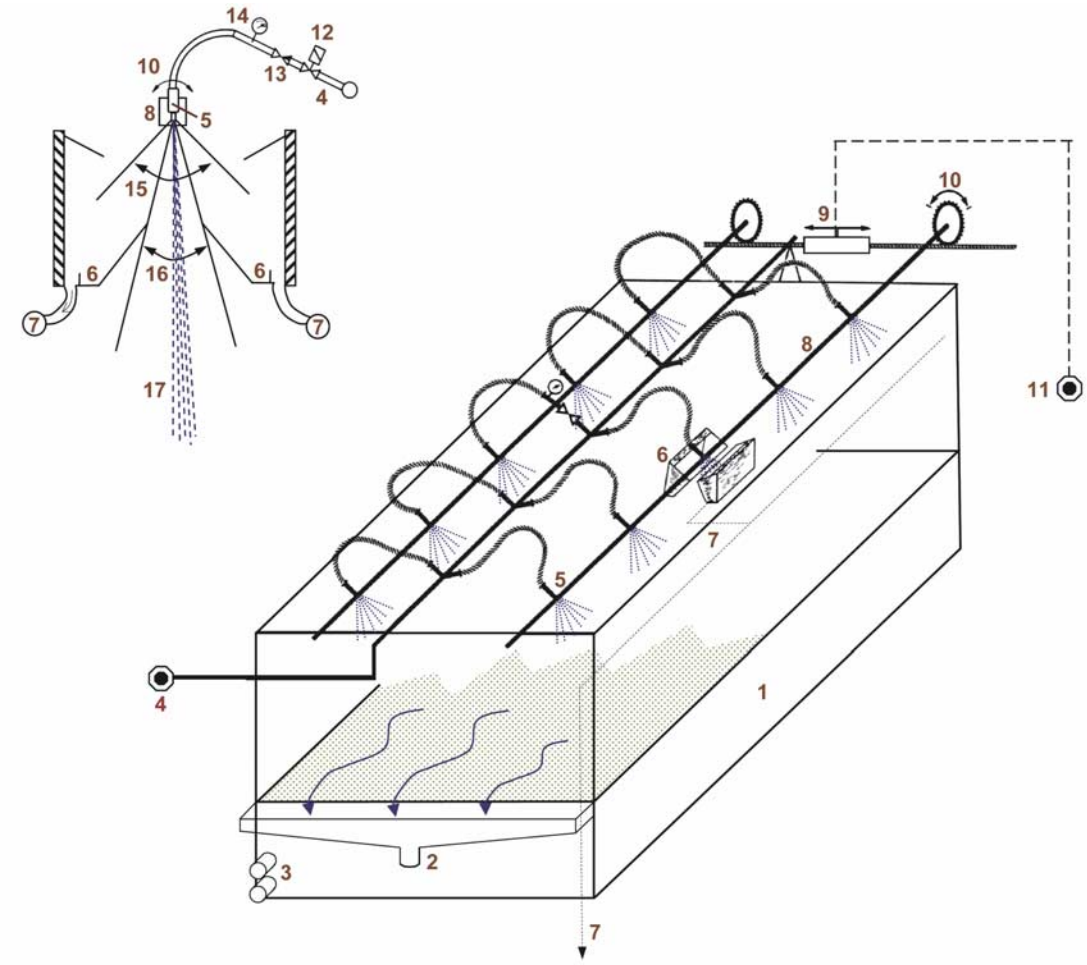

Figure 1. Overview of the experimental setup.

sediment samples using the pipette method (for silt and clay) and wet sieving (for sand) (Table 1). The size classes were <2, 2–20, 20–50, 50–100, 100–315, 315–1000, and >1000 μm. The eroded sediment rarely contained particles larger than 2500 μm. We used 10.0 g of the oven-dried sediment sample for the determination of the size class distribution. If there was less than 10.0 g of sediment in a sample, consecutive samples were combined and the composite sample was analyzed.

2.1.4. Overview of the Experiments

[12] We did 14 high rainfall intensity (47.5–52.5 mm/h) experiments on three different slopes (2.2, 7.2, and 12.4%) and two different loam soils (Table 1). Soil type 2 has a smaller clay and silt content and a larger sand and gravel content than soil 1 (Figure 2). The top 0.05–0.10 m of the soil surface was replowed, the largest pieces of gravel (>20 mm) were removed, and the soil surface was leveled at least 1 day prior to each experiment. Each experiment lasted at least 2 h (Table 1).

2.2. Model

2.2.1. Introduction

[13] We modified the analytical solutions of *Parlange et al.* [1999] to allow for infiltration. This approximation extended earlier work of *Hairsine and Rose* [1991] and decoupled the short-time and long-time behavior. The derivation presented here follows that of *Parlange et al.* [1999].

[14] The basic equations for soil erosion in overland flow have been described in detail elsewhere [e.g., *Hairsine and Rose*, 1991; *Sander et al.*, 1996]. Similar to *Parlange et al.* [1999] and *Sander et al.* [1996], we assume that the

Table 1. Overview of the High-Intensity Erosion Experiments on Reworked Soil With Vertical Drainage

Experiment	Soil Type	Duration, h	Slope, %	P, mm/h	f, mm/h	Number of Samples: Total Concentration	Number of Samples: Size Fractions
H1	1	2.33	2.2	47.5	7.6	41	30
H2	1	2.08	2.2	47.5	6.5	42	22
H3	1	2.17	2.2	47.5	3.2	41	21
H4	1	2.42	7.2	47.5	0.9	44	12
H5	1	2.52	7.2	47.5	1.7	40	16
H6	1	2.37	12.4	47.5	2.8	44	13
H7	1	2.23	2.2	47.5	2.1	42	16
H8	1	2.03	2.2	47.5	1.5	45	18
H9	2	2.00	7.2	50.0	2.0	41	15
H10	2	2.02	7.2	50.0	3.4	42	12
H11	2	2.10	7.2	50.0	1.5	41	14
H12	2	2.22	12.4	50.0	0.6	41	10
H13	1	2.07	12.4	52.5	0.6	41	13
H14	1	2.12	12.4	52.5	1.9	42	11

transport of sediment and water occurs in a strip of unit width down a plane surface and is shallow enough for the kinematic overland flow approximation to be valid. The equation for the conservation of sediment mass in particle size class i for this system can then be written as [*Sander et al.*, 1996]

$$\frac{\partial C_i}{\partial t} + \frac{q}{D}\frac{\partial C_i}{\partial x} = \frac{1}{D}(e_i - d_i + e_{di} - RC_i), \tag{1}$$

where t is time, x is the distance down the slope, C_i is the suspended sediment concentration of size class i, D is the depth of flow, q is the volumetric flux per unit width of the plane, R is the excess rainfall rate, e_i is the rainfall detachment rate of size class i from the original bare soil, d_i is the deposition rate of suspended sediment of size class i, and e_{di} is the redetachment rate of deposited material of size class i. The deposition rate is proportional to the net settling velocity of size class i and thus varies by many orders of magnitude:

$$d_i = (V_i + f)C_i, \tag{2}$$

where V_i is the settling velocity (due to gravity) of size class i and f is the infiltration rate. Assuming that rainfall detachment is nonselective with respect to size class i and that the deposited material will shield some fraction of the original soil (H), the detachment rate can be described by

$$e_i = \frac{aP}{I}[1 - H(t,x)], \tag{3}$$

where P is the rainfall rate, a is the rainfall detachability of the original bare soil, and I is the total number of size classes ($\sum i$). Precipitation and the excess rainfall rate are related according to

$$R = P - f. \tag{4}$$

The distribution of particles in the deposited layer is size-dependent due to the size dependence of the deposition rate (2). Therefore the redetachment rate can be described as

$$e_{di} = a_d P \frac{M_{di}}{M_{dt}} H(t,x), \tag{5}$$

where a_d is the detachability of the deposited layer, M_{di} is the mass per unit area of sediment of size class i in the deposited layer, and M_{dt} is the total mass of sediment in the deposited layer ($\sum_{i=1}^{I} M_{di}$). Mass conservation for the deposited layer is given by

$$\frac{\partial M_{di}}{\partial t} = d_i - e_{di}, \tag{6}$$

as only deposition and redetachment affect the deposited layer.

[15] Defining the mass per unit area needed for complete shielding as M_{dt*} gives

$$H(t,x) = \frac{M_{dt}}{M_{dt*}}. \tag{7}$$

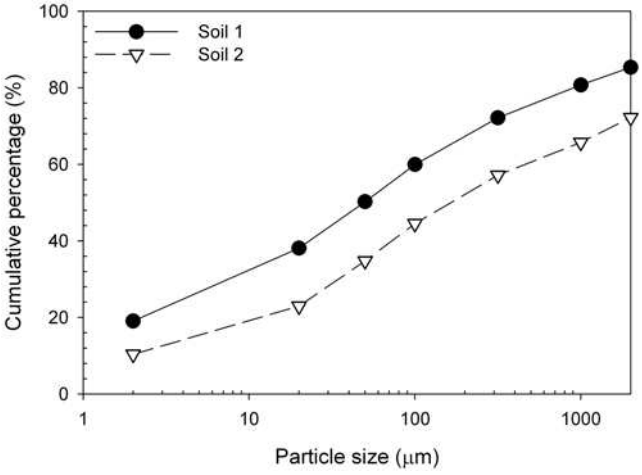

Figure 2. Comparison of the grain size distributions of the two soil types.

[16] Using the following dimensionless parameters:

$$b = \frac{P}{R},\ \tau = \frac{Rt}{D},\ c_i = \frac{C_i}{ab},\ m_{di} = \frac{M_{di}}{abD},\ v_i = \frac{V_i + f}{R},$$
$$K = \frac{a_d}{a},\ \alpha = \frac{a_d bD}{M_{dt}*},$$

and assuming that (1) the spatial gradients in the sediment concentration are small compared with the temporal gradients and (2) the water depth is independent of space and time allows one to rewrite (1)–(7) as

$$\frac{d(c_i + m_{di})}{d\tau} = \frac{1 - H}{I} - c_i, \tag{8}$$

$$\frac{dm_{di}}{d\tau} = v_i c_i - \alpha m_{di}, \tag{9}$$

$$H = \frac{\alpha}{K} \sum_{i=1}^{I} m_{di}. \tag{10}$$

Note that these equations are identical to (7)–(9) of *Parlange et al.* [1999] albeit with different dimensionless parameters since here infiltration is considered (i.e., $P \neq R$). The dimensionless parameter v_i now includes, in addition to the settling velocity due to gravity (V_i), the vertical flow component due to infiltration (f). This parameter thereby describes the behavior of the net settling velocity. Inclusion of f mainly influences the net settling velocity of the smallest particles for which f is of the order of or larger than the settling velocity due to gravity (V_i).

[17] Since (8)–(10) are identical to the equations given by *Parlange et al.* [1999] the derivations of the short-time and long-time solutions are identical to those described by *Parlange et al.* [1999] and therefore not given here.

2.2.2. Short-Time Behavior

[18] The short-time solution is given by *Parlange et al.* [1999]

$$c_i = \frac{\alpha}{\alpha + v_i} F, \tag{11}$$

where F is equal to

$$F = \frac{K}{\alpha \sum_{i=1}^{I} \frac{v_i}{\alpha + v_i}} \left[1 - \exp\left(-\frac{\alpha}{IK} \sum_{i=1}^{I} \frac{v_i}{\alpha + v_i} \tau \right) \right]. \tag{12}$$

[19] The fraction of shielding is

$$H = 1 - \exp\left(-\frac{\alpha}{IK} \sum_{i=1}^{I} \frac{v_i}{\alpha + v_i} \tau \right), \tag{13}$$

which is independent of space following the assumptions above (8).

2.2.3. Long-Time Behavior

[20] An expression for the long-time behavior is also given by *Parlange et al.* [1999]. However, here we introduce two additional simplifications. First, we assume that the fraction of shielding (H) has already reached the steady state value when the long-time solution applies. Second, we assume that $IK \ll \sum_{i=1}^{I} v_i$. These assumptions will be checked subsequently (section 3.3).

[21] The sediment concentration at steady state (i.e., infinite time) (c_{if}) is independent of size class and is equal to

$$c_{if} = \frac{1 - H(\tau \to \infty)}{I}, \tag{14}$$

where $H(\tau \to \infty)$ is the fraction of shielding at steady state, which is equal to

$$H(\tau \to \infty) = \frac{\sum_{i=1}^{I} v_i}{IK + \sum_{i=1}^{I} v_i}. \tag{15}$$

The second assumption allows us to rewrite the concentration at steady state (14) as

$$c_{if} = \frac{K}{\sum_{i=1}^{I} v_i}. \tag{16}$$

Combined with the first assumption, this allows us to rewrite the solution for the long-time behavior as

$$c_i = c_{if} + (c_{io} - c_{if}) \exp(-l_i \tau), \tag{17}$$

where c_{io} is the "initial" concentration of the long-time behavior:

$$c_{io} = \frac{K}{(\alpha + v_i) \sum_{i=1}^{I} \frac{v_i}{\alpha + v_i}} \tag{18}$$

$$l_i = \frac{\alpha}{\alpha + v_i}. \tag{19}$$

The combined behavior is obtained by using the uniform approximation (i.e., multiplying the long-time concentrations (17) by the short-time fraction of shielding (13)) [*Parlange et al.*, 1999].

2.2.4. Model Application and Parameter Estimation

[22] In order to be able to test the analytical solutions to the Hairsine-Rose model one has to assume that rainfall driven interrill soil erosion was the dominant erosion mechanism. We did not observe any rill formation during the experiments suggesting that rill erosion did not occur. Flow-driven erosion was likely unimportant during the low slope experiments but could have become more important during the higher slope experiments.

[23] For the model application, the soils in the erosion flume were divided into 40 size classes (I = 40) of equal mass. After calculating the sediment concentrations for each of these 40 classes, these size classes were regrouped into seven classes (which did not have equal mass) to allow for

Table 2. Overview of the Seven Particle Size Diameter Classes With the Corresponding Calculated or Measured Settling Velocities and the Optimized Multiplication Coefficients for the Settling Velocities

	Diameter, μm		Settling Velocity (V_i), m/s		Number of Size Class (i)		Multiplication Coefficient for the Settling Velocity (k_{vi})
Size Class (s)	From	To	From	To	Soil 1	Soil 2	
1	0	2	8.0×10^{-8}	4.0×10^{-6}	9	6	3.5
2	2	20	4.0×10^{-6}	4.0×10^{-4}	9	7	4.5
3	20	50	4.0×10^{-4}	2.5×10^{-3}	5	6	9.0
4	50	100	2.5×10^{-3}	1.4×10^{-2}	5	6	8.5
5	100	315	1.4×10^{-2}	3.7×10^{-2}	5	6	1.5
6	315	1000	3.7×10^{-2}	6.9×10^{-2}	4	5	0.70
7	>1000		6.9×10^{-2}	1.4×10^{-1}	3	4	0.35

the comparison with the observed data (Table 2). *Sander et al.* [1996] found that I had to be at least 10 in order to be able to represent the underlying physics of the erosion processes and the structure of the experimental data. We used a larger number of size classes in order to be able to later regroup them according to the analyzed size classes.

[24] The analytical solutions assume steady state hydrological conditions (i.e., a steady infiltration and excess rainfall rate). Thus we used the measured steady state excess rainfall rate (R) (reached within several minutes of the start of overland flow). The infiltration rate was then calculated as the difference between the rate of water application (P) and the steady state excess rainfall rate (4). This resulted in a constant infiltration rate (f) that was then used in the analytical solutions.

[25] Since we do not know the value of the detachability of the original bare soil (a) or the detachability of the deposited layer (a_d), we had to optimize the values of the aK, K, and α parameters. Even if we could have estimated the detachabilities of the soil and the deposited layer, the estimate of their ratio (K) would be uncertain. Also, because of the low water depth and spatial variation in water depth across the flume due to the roughness of the soil surface, it was not possible to measure the effective water depth (D). Therefore we optimized this parameter as well. However, we checked that the optimized value was within the estimates made during the experiments (i.e., less than 20 mm).

[26] The optimized values of aK, K, α, and D were found by minimizing the sum of the sum of the absolute errors, E_{abs}, for all seven observed size classes:

$$E_{abs} = \sum_{s=1}^{7} \sum_{n=1}^{N} |C_{\text{obs\_s}} - C_{\text{mod\_s}}|, \tag{20}$$

where s is the size class, N is the number of samples, $C_{\text{obs\_s}}$ is the observed concentration of size class s, and $C_{\text{mod\_s}}$ is the predicted concentration of size class s. To determine the sensitivity of the model to the optimized parameter values and the definability of the parameters, we did a series of Monte Carlo simulations that are described in more detail in section 3.4.

[27] For the three smallest size classes (<2, 2–20, and 20–50 μm) we used the Stokes' settling velocity [*Stokes*, 1851] because we could not measure the settling velocities for these particles and because the pipette method used for the analysis of these particle sizes also assumes Stokes' settling velocities. For the four largest particle size classes (50–100, 100–315, 315–1000, and >1000 μm) we used the average of the settling velocities measured in a 0.47-m-long tube filled with tap water for each size class. Stokes settling velocities were not used for these particles because the Stokes settling equation does not hold for particles larger than ~60 μm [*Childs*, 1969] and because roundness and shape effects result in a smaller settling velocity for natural sediments compared with spheres [*Baba and Komar*, 1981; *Dietrich*, 1982; *Jiménez and Madsen*, 2003; *Tomkins et al.*, 2005]. The measured settling velocities were smaller than those calculated if the Stokes' settling velocity was used, larger than those calculated using the *Gibbs et al.* [1971] empirical equation, and of the same order of magnitude as those calculated with the *Dietrich* [1982] and *Ferguson and Church* [2004] equations.

3. Results

3.1. Experimental Results

[28] Total sediment concentrations and the concentrations of the smallest size fractions (<20 μm) increased quickly after the onset of overland flow. The midsize size fractions (20–100 μm) had a more attenuated response. There was more scatter in the data for the largest size fractions (>100 μm). The concentrations of the largest size fractions were either very low initially and increased gradually over the course of the experiment or remained nearly constant (with a high variability) throughout the experiment (Figure 3). The very long time (steady state) concentrations resembled the composition of the soil in the erosion flume (Figure 3).

3.2. Model Results

[29] The new simplifications for the multiple particle size class sediment transport equations and the inclusion of infiltration worked well for the total sediment concentration. However, the optimized parameter sets led to a significant underestimation of the concentrations of the largest size classes (315–1000 and >1000 μm) and an underestimation of the steady state concentrations for all size classes (Figure 3). When the parameters were found by minimizing the sum of the absolute errors for total concentration (rather than the sum of the sum of the absolute errors for all seven size classes (equation (20)), the total sediment concentration could be very well predicted, the steady state total sediment concentration was no longer underestimated, and the concentrations for the largest size classes (315–1000 and

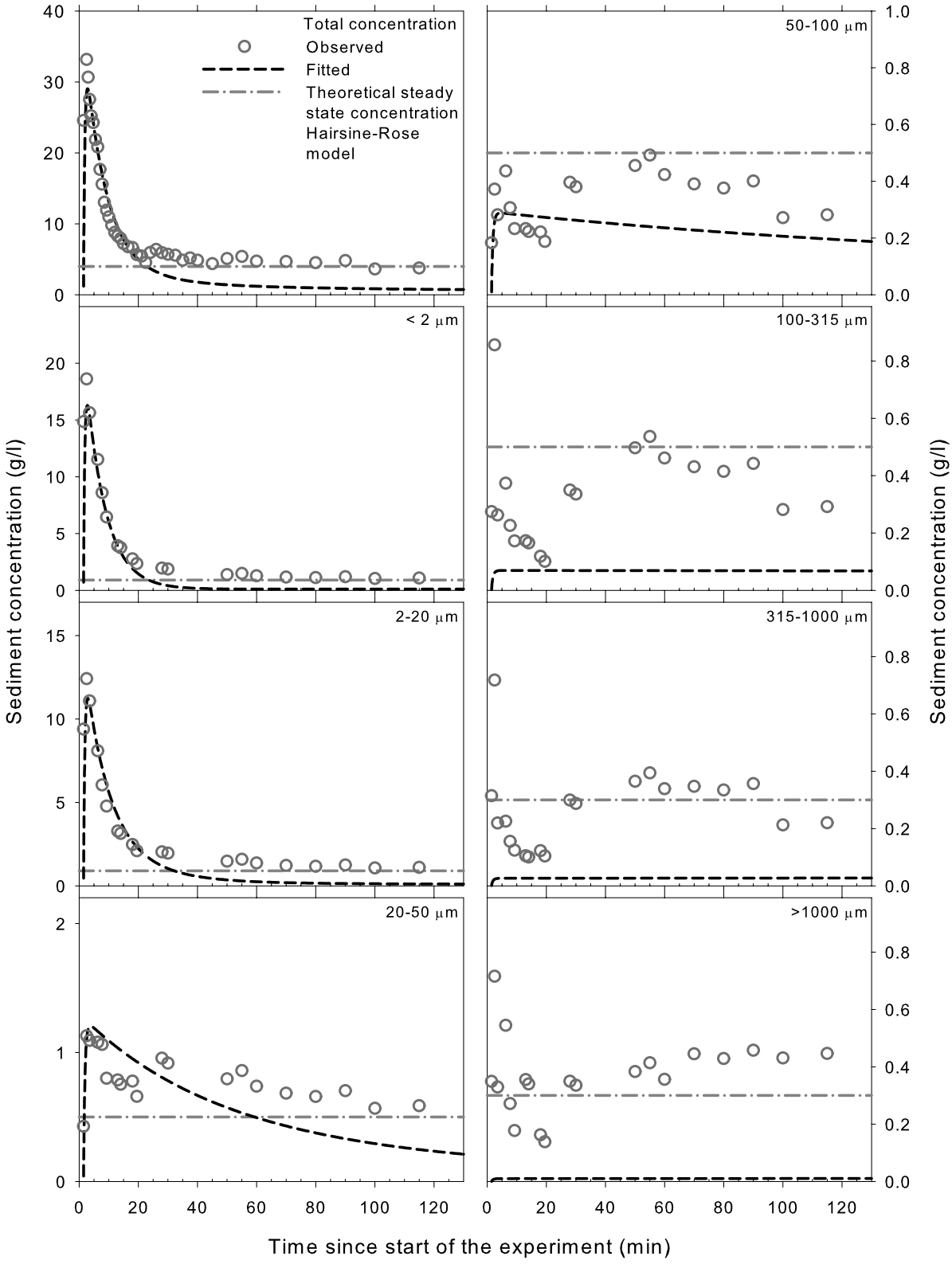

Figure 3. Observed concentrations and fitted concentrations for experiment H3 found by minimizing the sum of the sum of absolute errors for the seven size classes (20). The theoretical steady state concentrations of the Hairsine-Rose model, representing the original soil composition, are shown as well. The results shown here for experiment H3 are typical for all other experiments. Parameters are aK = 582 mg/cm^3, α = 11, D = 4.8 mm, and K = 0.5.

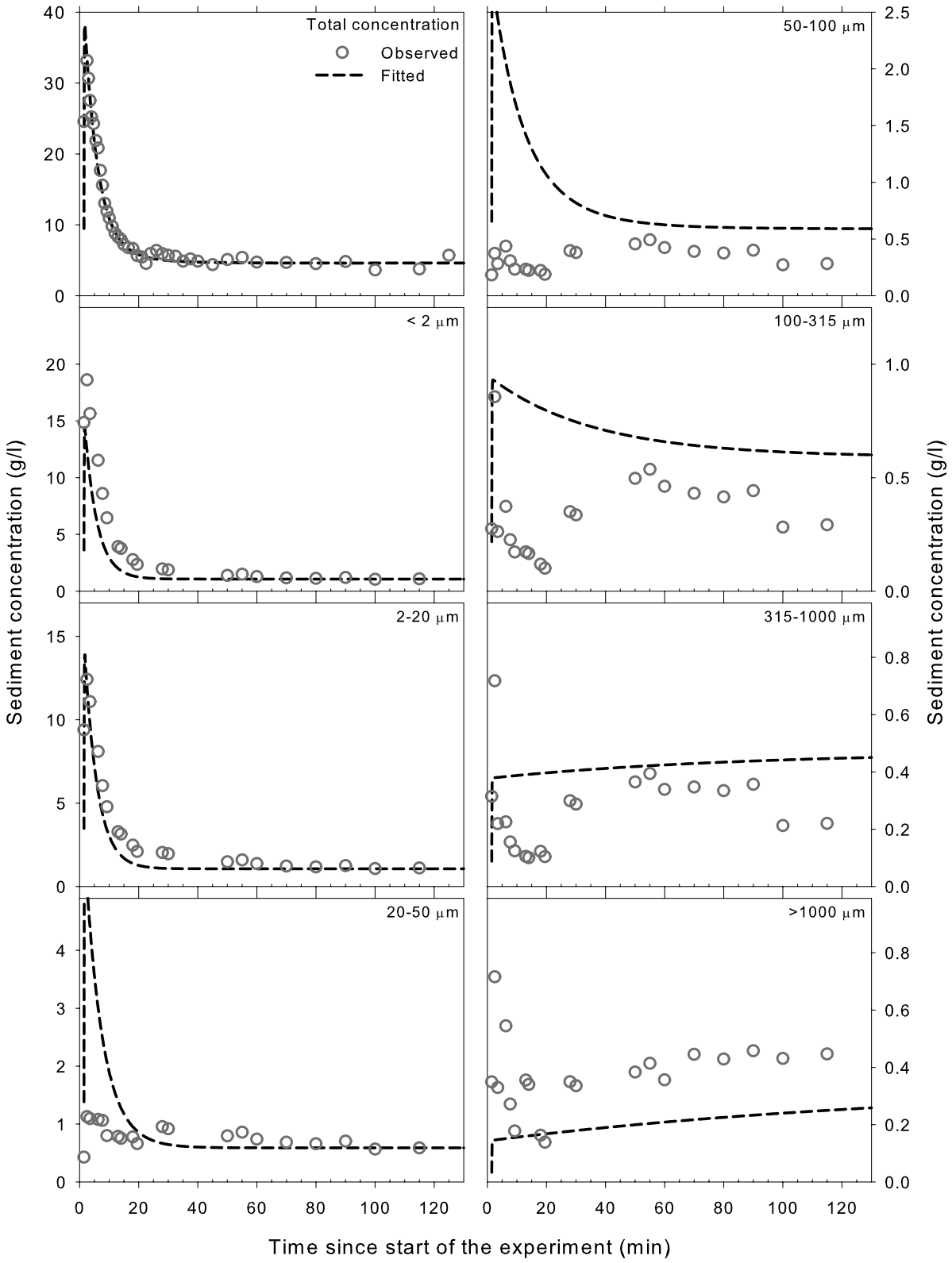

Figure 4. Observed and fitted concentrations for experiment H3 found by minimizing the sum of the absolute errors for the total sediment concentration. The results shown here for experiment H3 are typical for all other experiments. Parameters are aK = 5890 mg/cm^3, α = 223, D = 3.1 mm, and K = 1.4.

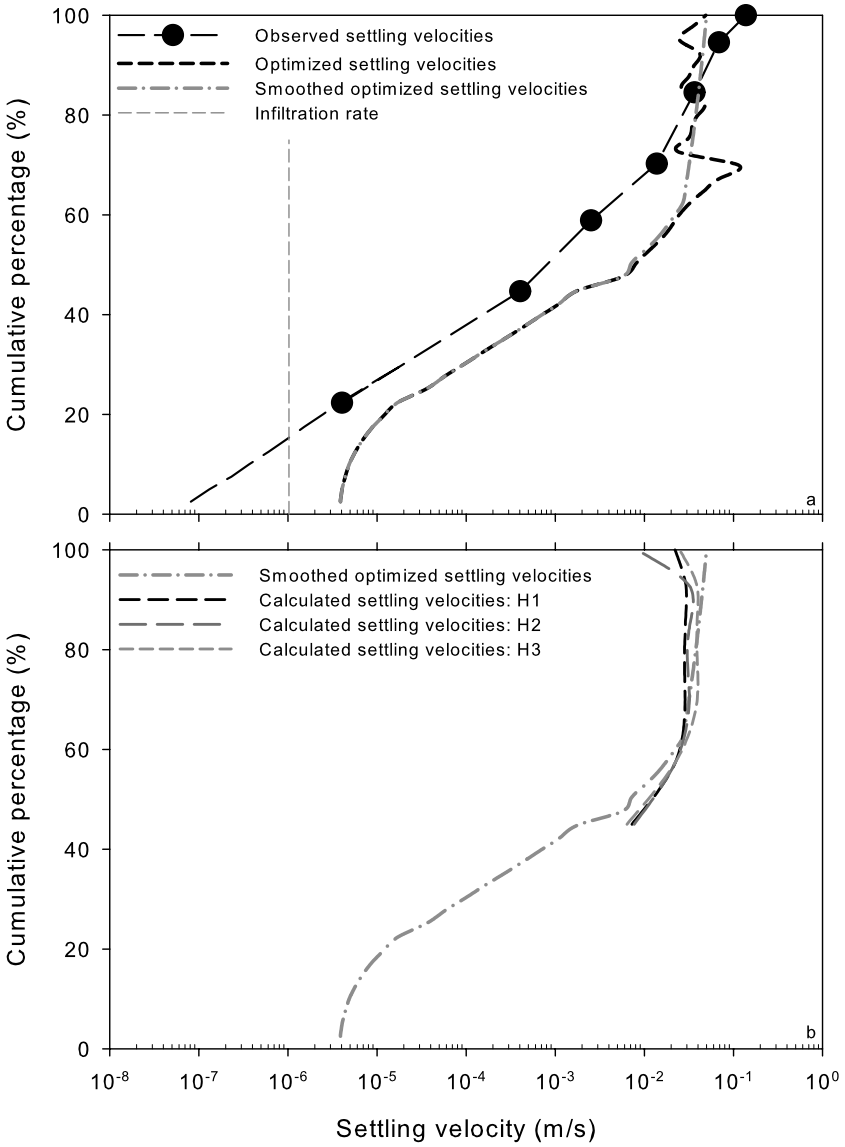

Figure 5. (a) Observed and optimized settling velocities for experiment H3 and (b) the smoothed optimized settling velocities for experiment H3 and the calculated settling velocities from the ratios of the amount of sediment in the shield for experiments H1, H2, and H3. The results shown here are typical for all experiments.

>1000 μm) were less underestimated. However, with this optimized parameter set the peak concentrations for the midsize classes (20–50 μm and 50–100 μm) were very much overestimated (Figure 4). The model predicted that the midsize classes behaved like the smaller particles, having a high peak concentration and declining quickly to a steady state concentration rather than the observed attenuated peak or slow increase toward the steady state concentration.

[30] Both parameter optimization procedures (minimizing the sum of the sum of the absolute errors for the concentrations of the seven observed size classes and minimizing the sum of the absolute errors for the total concentration) as well as manual (visual) optimization resulted in parameter sets that either significantly underestimated the steady state concentrations and the concentrations of the largest size classes (315–1000 and >1000 μm) or overestimated the peak concentrations of the midsize classes (20–50 and 50–100 μm) and still underestimated the concentrations of the largest size classes (Figures 3 and 4). While the large size classes do not contribute significantly to the peak total sediment concentration, they do contribute to the steady state total sediment concentration and the sediment size distribution at the end of the experiments. Further investigation revealed that these large size classes had measured settling velocities that led the model to predict their almost immediate settling, whereas the data did not show this. To overcome this deficiency, we multiplied the dimensionless settling velocities of each observed size class by a multiplication coefficient (k_{vi}). In order to gain insight into the processes controlling the experimental data, we manually optimized the multiplication coefficients for experiment H3. This high-intensity, low slope experiment was chosen because of the large number of sediment samples that were taken during this experiment (Table 1) and its representative

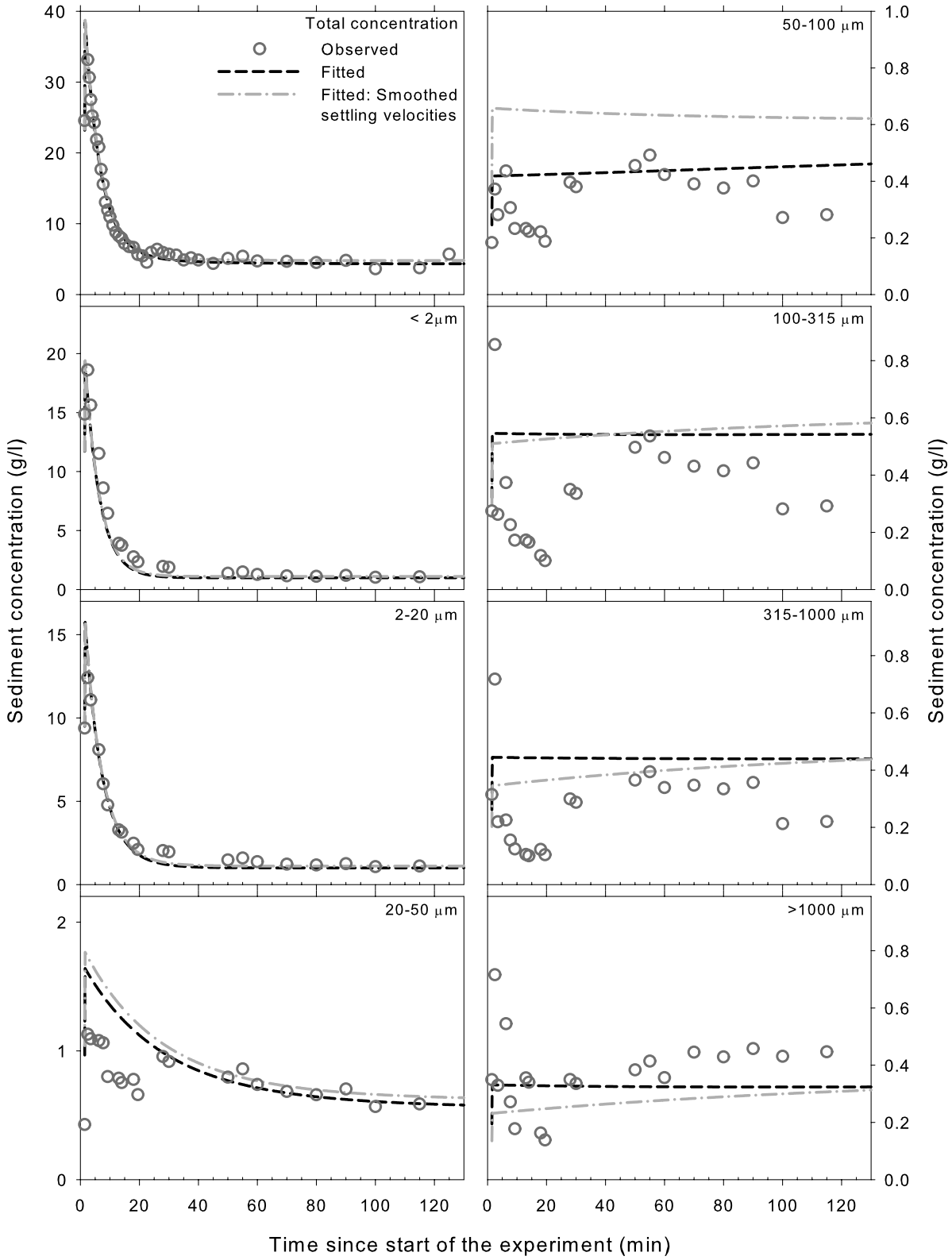

Figure 6. Observed and fitted concentrations for experiment H3. The parameters were found by minimizing the sum of the sum of the absolute errors for the individual size classes (20). The multiplication coefficients for the settling velocities were manually optimized (Table 2). The results using the smoothed distribution of settling velocities (Figure 5) are shown as well. The results shown here for experiment H3 are typical for all other experiments. Parameters are aK = 6510 mg/cm^3, α = 142, D = 3.6 mm, and K = 0.30.

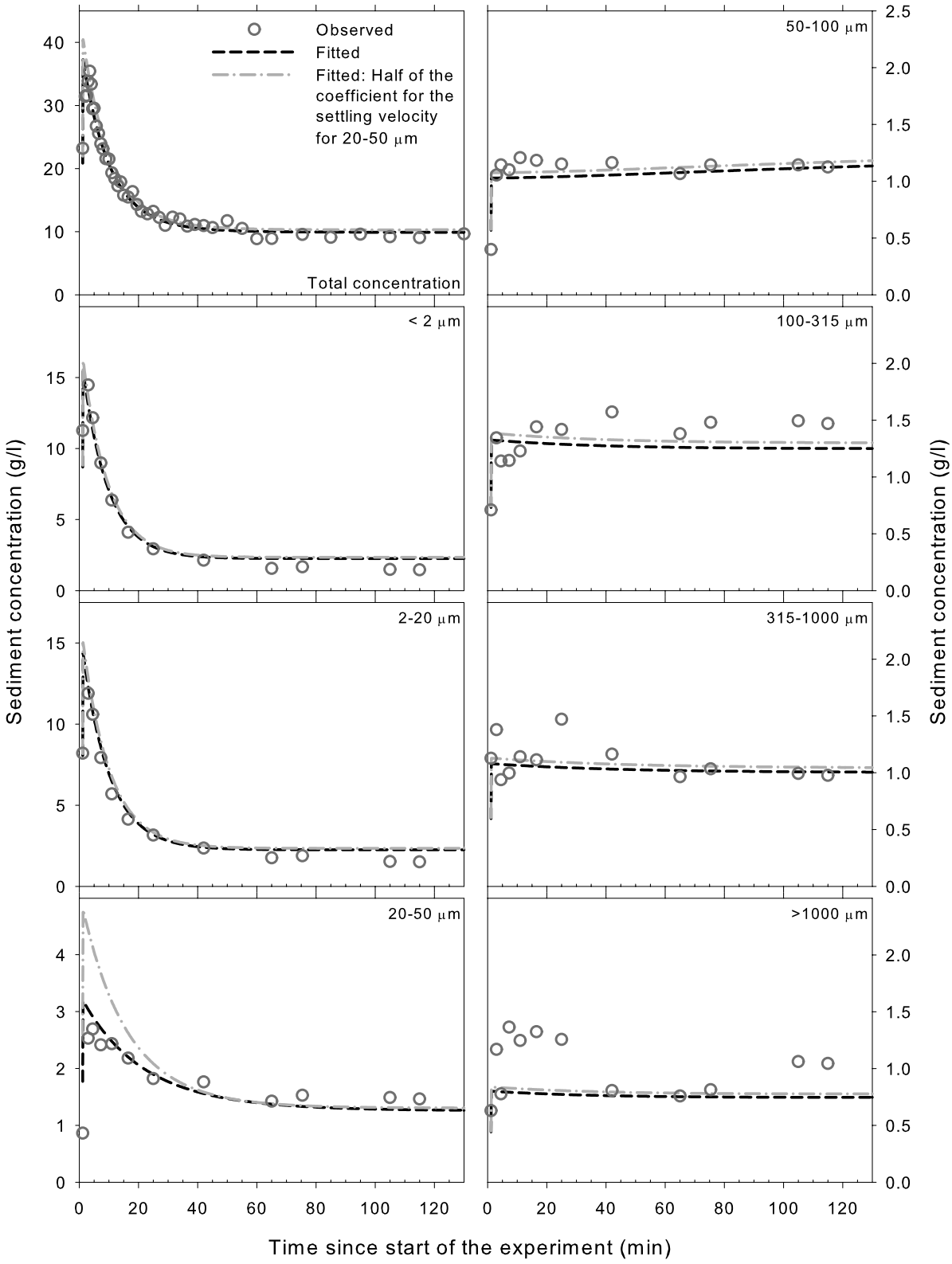

Figure 7. Observed and fitted concentrations for experiment H4. The parameters were found by minimizing the sum of the sum of the absolute errors for the individual size classes (20). The multiplication coefficients for the settling velocities from experiment H3 were used. The results for a simulation with a multiplication coefficient of 4.5 (half of the optimized value) for the 20–50 μm size class are shown as well. The results shown here for experiment H4 are typical for all other experiments. Parameters are aK = 14,742 mg/cm^3, α = 470, D = 6.6 mm, and K = 0.5.

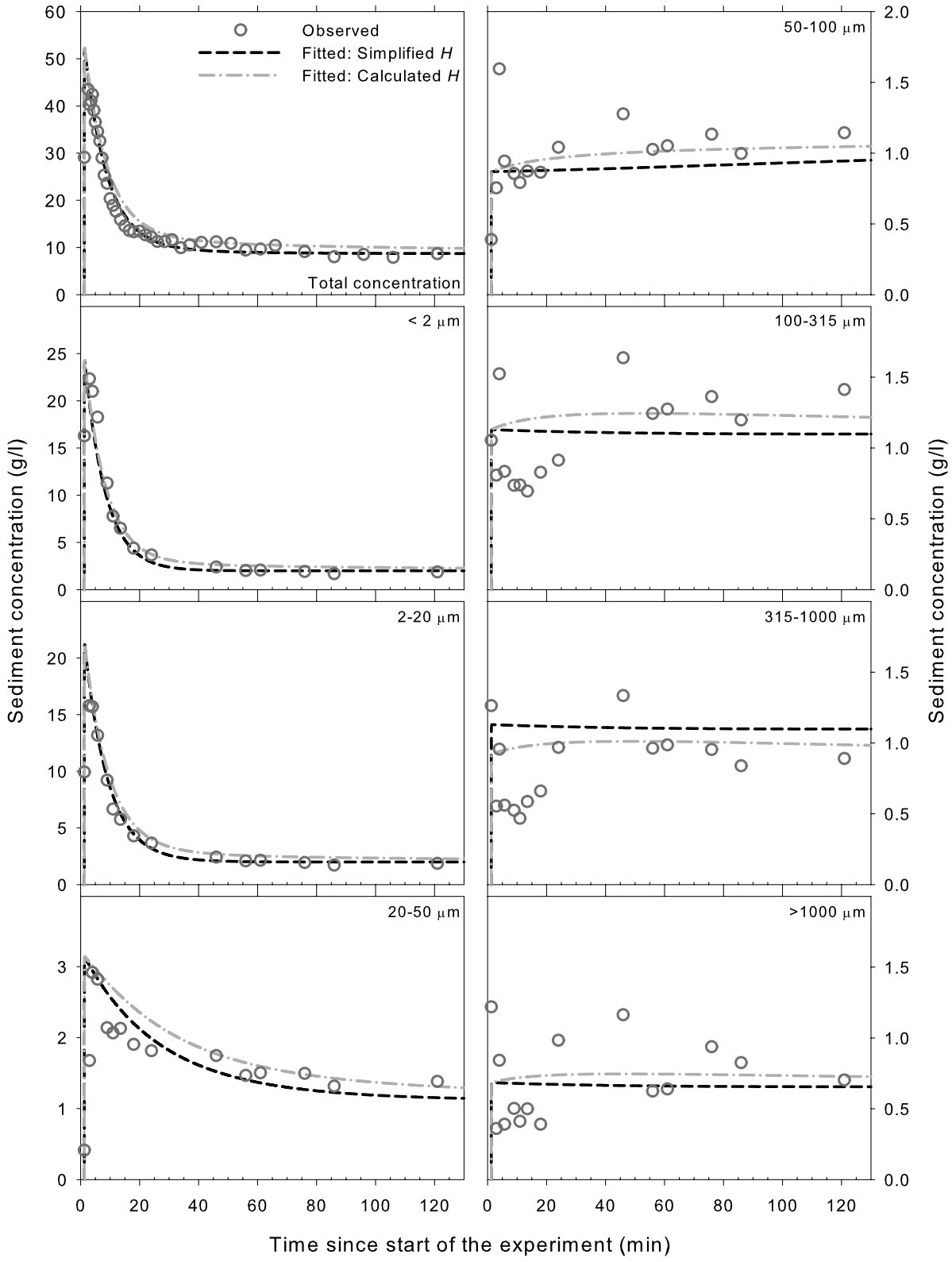

Figure 8. Comparison of the calculated sediment concentrations using the late time shielding fraction (H) given by *Parlange et al.* [1999] and the sediment concentrations calculated using the shielding fraction at infinite time (i.e., the simplification used in this study) for experiment H5. The results shown here for experiment H5 are typical for all other experiments. Parameters are aK = 13,040 mg/cm^3, α = 240, D = 5.3 mm, and K = 0.3.

Table 3. Overview of the Average Absolute Error $(1/N)\sum_{i=1}^{N}|C_{obs\_s}-C_{mod\_s}|$ and the Average Relative Error $(1/N)\sum_{i=1}^{N}|(C_{obs\_s}-C_{mod\_s})/C_{obs\_s}|$ (in Parentheses), Where C_{obs_s} is the Observed Concentration of Size Class s, C_{mod_s} is the Calculated Concentration of Size Class s, and N is the Number of Measurements

Experiment	Total Concentration	Size Class, μm						
		<2	2–20	20–50	50–100	100–315	315–1000	>1000
H1	1.05 (0.18)	0.83 (0.31)	0.58 (0.25)	0.23 (5.16)	0.04 (0.29)	0.06 (0.46)	0.07 (0.64)	0.13 (0.98)
H2	1.07 (0.12)	1.17 (0.30)	0.49 (0.19)	0.35 (0.65)	0.04 (0.14)	0.11 (0.33)	0.12 (0.54)	0.23 (0.39)
H3	0.76 (0.09)	1.13 (0.24)	0.42 (0.16)	0.24 (0.30)	0.11 (0.42)	0.23 (1.10)	0.20 (1.21)	0.11 (0.32)
H4	0.96 (0.06)	0.81 (0.22)	0.52 (0.17)	0.23 (0.15)	0.08 (0.08)	0.16 (0.12)	0.16 (0.13)	0.29 (0.25)
H5	1.26 (0.08)	1.08 (0.11)	0.50 (0.09)	0.34 (0.35)	0.16 (0.15)	0.30 (0.30)	0.24 (0.33)	0.24 (0.38)
H6	1.98 (0.10)	0.97 (0.25)	0.67 (0.18)	0.28 (0.14)	0.40 (0.20)	0.42 (0.18)	0.24 (0.17)	0.30 (0.41)
H7	2.14 (0.10)	4.42 (0.44)	2.60 (0.26)	0.55 (0.76)	0.13 (0.63)	0.23 (1.84)	0.21 (2.18)	0.21 (1.91)
H8	0.89 (0.10)	1.08 (0.28)	0.68 (0.23)	0.26 (0.51)	0.06 (0.21)	0.15 (0.43)	0.15 (0.53)	0.18 (1.50)
H9	0.83 (0.07)	1.46 (0.42)	0.60 (0.14)	0.84 (0.60)	0.11 (0.21)	0.25 (0.53)	0.19 (0.52)	0.16 (0.75)
H10	0.85 (0.06)	1.13 (0.30)	0.50 (0.13)	0.75 (0.47)	0.19 (0.22)	0.32 (0.34)	0.18 (0.28)	0.22 (0.55)
H11	1.40 (0.11)	0.70 (0.19)	0.39 (0.12)	0.41 (0.30)	0.13 (0.17)	0.28 (0.41)	0.24 (0.49)	0.34 (0.43)
H12	1.32 (0.07)	0.73 (0.14)	0.67 (0.15)	0.51 (0.20)	0.57 (0.24)	0.73 (0.25)	0.48 (0.21)	0.25 (0.25)
H13	2.22 (0.08)	2.88 (0.31)	2.90 (0.33)	0.99 (0.15)	1.52 (0.38)	1.67 (0.34)	1.04 (0.28)	0.71 (0.44)
H14	2.57 (0.10)	2.71 (0.30)	3.24 (0.42)	0.90 (0.20)	1.04 (0.26)	1.14 (0.23)	0.85 (0.28)	0.51 (0.24)

behavior. The optimized multiplication coefficients were larger than unity for the five smallest size classes (<2, 2–20, 20–50, 50–100, and 100–315 μm) but smaller than unity for the two largest size classes (315–1000 and >1000 μm) (Table 2). Thus the optimum settling velocities were larger than the measured or calculated settling velocities plus the infiltration rate for the five smallest size classes but smaller than the measured settling velocities for the two largest size classes (Figure 5). Figure 5 suggests that there is a maximum settling velocity of $\sim 3 \times 10^{-2}$ m/s for all particles >100 μm.

[31] We then used these optimized multiplication coefficients from experiment H3 for all the other experiments. This adjustment of the settling velocities resulted in very good fits for both the total sediment concentrations and the concentrations of the individual size classes for all experiments (Figures 6–8, Table 3). The calculated total sediment concentrations and the calculated concentrations for the individual size classes were not very sensitive to the exact value of the multiplication coefficients for the settling velocities (Figures 6 and 7). The sediment concentrations of the individual size classes calculated using the optimized multiplication coefficients (Table 2), and those calculated using a smooth settling velocity distribution (Figure 5a) were very similar (Figure 6).

[32] A second method to obtain the settling velocities is to optimize the settling velocity for only one of the size classes and to obtain the settling velocity distribution from the distribution of material in the shield. The Hairsine-Rose model states that at steady state the amount of material in the shield of each individual size class (m_{di}) is directly proportional to the settling velocity of that size class (v_i) [see, e.g., *Parlange et al.*, 1999, equation 29]. We calculated the amount of material in the shield for each of the size classes from the experimental data by assuming that none of the sediment <2 μm is in the shield and that detachment is nonselective with respect to size. The measurement of the amount of sediment <2 μm leaving the flume tells us how much of the original soil has been eroded in each class size (since we know the particle size distribution of the original soil), and by subtracting the measured amount of sediment in each size class leaving the flume, we know their amount in the shield. Further, assuming that we know the settling velocity for the $\sim$50-μm particles (i.e., for i = 23) (here chosen based on the optimized settling velocity as 2.25×10^{-2} m/s), we could calculate the settling velocities from the observed data. These settling velocities agreed very well with the optimized settling velocities (Figure 5b).

3.3. Consistency of the Simplifying Assumptions for the Long-Time Behavior

[33] The discrepancy between the long-time shielding fraction and the shielding fraction at steady state was small and decreased with time (e.g., 0.99965 versus 0.99979 at 5 min, and 0.99967 versus 0.99979 at 10 min after the start of overland flow for experiment H5). The influence of this difference on the predicted sediment concentrations was also small (Figure 8). The simplifying assumption for the calculation of the long-time concentrations resulted in a somewhat sharper increase in sediment concentrations for the large particles and a somewhat sharper decrease in sediment concentrations for the smaller particles (Figure 8).

[34] The sum of the optimized settling velocities $(\sum_{i=1}^{I} v_i)$ ranged from 5×10^4 to 7×10^4. Since the optimized value of K was never larger than 10 for the experiments in this study and I was 40, it is clear that indeed $IK \ll \sum_{i=1}^{I} v_i$ and that the second simplifying assumption is valid as well.

3.4. Parameter Definability

[35] We did 75,000 Monte Carlo simulations with the adjusted settling velocities for each experiment to determine how well defined the model parameters are. The parameter range was set from 1 to 35,000 for aK, from 1 to 1500 for α, from 1 to 20 mm for D, and from 0.01 to 100 for K. The results of these simulations showed that aK, α, and D were very well defined for all experiments but that K was sometimes poorly defined (Figure 9). Also, aK was well defined for the total sediment concentration and the concentrations of all individual size classes. Its optimal value was similar for each size class. Both α and D were well defined for the total concentration and the smallest size

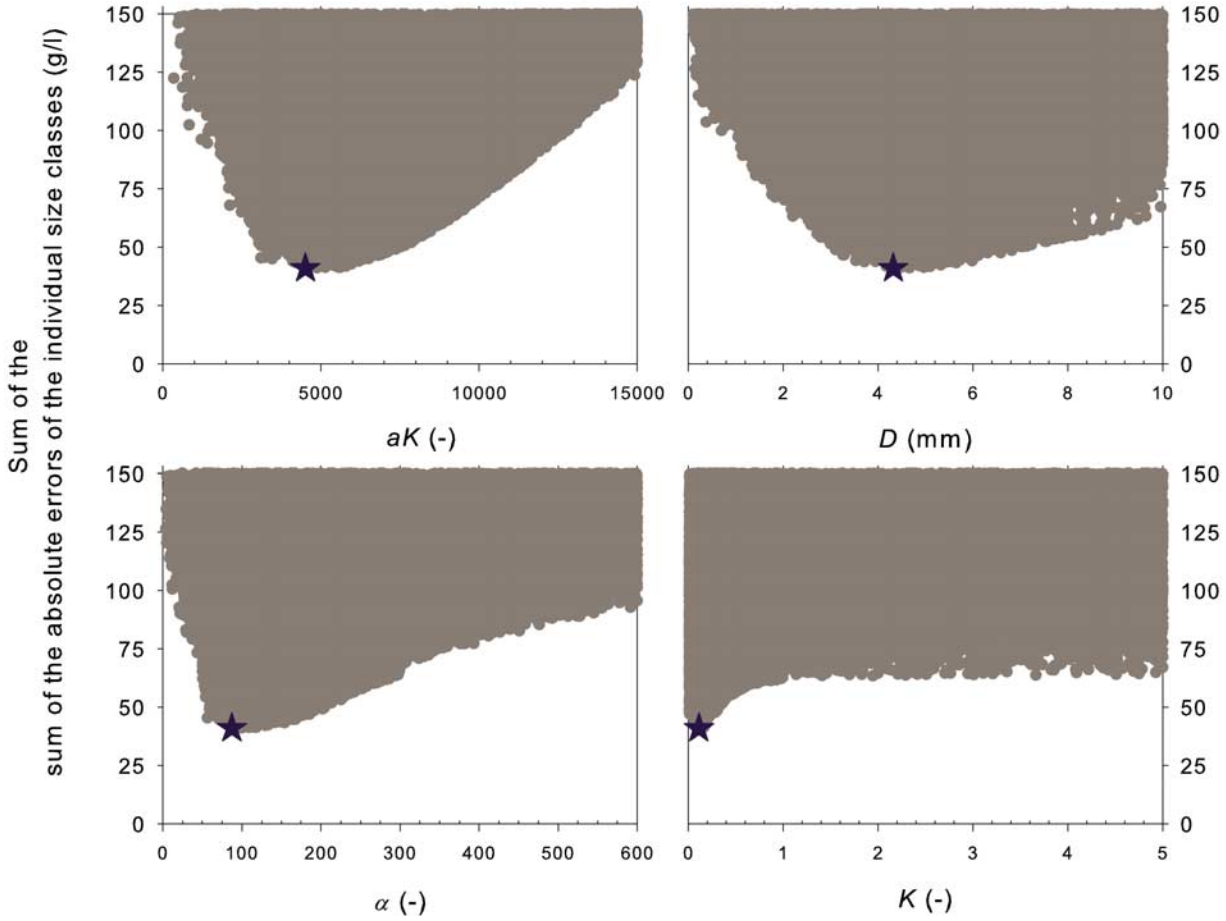

Figure 9. Results of 75,000 Monte-Carlo simulations to obtain the model parameters for experiment H3 with the optimized multiplication fractions for the settling velocities. The star represents the simulation with the lowest sum of the sum of absolute errors (20). The results shown here for experiment H3 are typical for all other experiments.

classes (<20 μm) but not for the larger size classes. When K was well defined, it was also well defined only for the smallest size classes but not for the larger size classes.

[36] While the Hairsine-Rose model is physically based, it was found that the optimal parameter values were different for each experiment and were somewhat related to the antecedent moisture conditions and slope. A more careful analysis of the behavior of the optimized parameter values is beyond the scope of this paper but will be done in a later study.

4. Discussion

4.1. Application of the Analytical Solutions

[37] The analytical solutions for rainfall-induced soil erosion could represent the total sediment concentration well, similar to the results of *Sander et al.* [1996] and *Parlange et al.* [1999]. However, the sediment concentrations of the individual size classes could not be represented when the calculated or measured settling velocities were used. *Sander et al.* [1996] and *Parlange et al.* [1999] did not show how well the numerical or analytical solutions represented the individual size classes.

[38] The analytical solutions could represent the experimental results of all size classes very well when adjusted settling velocities were used. The multiplication coefficients for the settling velocities were found via (manual) optimization, but could have been found from the calculated distribution of material in the shield as well when only one of the settling velocities was known or optimized. The four smallest size classes (<2, 2–20, 20–50, and 50–100 μm) and in particular the 20–50 and 50–100 μm size classes had optimized net settling velocities larger than the measured or calculated settling velocities plus the downward velocity component due to infiltration. The two largest size classes (315–1000 and >1000 μm) had optimized settling velocities that were smaller than the settling velocities measured in a tube filled with tap water, and were smaller than those calculated with the equations for settling velocity of *Dietrich* [1982] and *Ferguson and Church* [2004], but larger than those calculated with the empirical *Gibbs et al.* [1971] equation. Figure 5 suggests that there was a maximum settling velocity of $\sim 3 \times 10^{-2}$ m/s for all particles >100 μm. The range of settling velocities was thus smaller than calculated or measured (Figure 5a). The model was not very sensitive to the exact value of the multiplication coefficients for the settling velocities (Figures 6 and 7). The adjustment coefficients had the largest influence on the modeled concentrations of the largest particles (>100 μm) and a smaller effect on the modeled concentrations of the

smaller particles (<100 μm). For the smaller particles the adjustment coefficient mainly influenced the steady state concentrations, showing the importance of long duration experiments for the testing of erosion models.

[39] *Beuselinck et al.* [2002] developed a multiclass net deposition in overland flow equation based on the Hairsine-Rose theory. Their model could represent the total sediment flux at the end of a 2.6-m-long flume well but tended to overestimate the export of fines and underestimate the export of the coarser sediment. The underestimation of the export of coarse particles was attributed to sediment rolling over the flume bed. Their settling velocities were estimated from the particle diameter using the algorithm of *Dietrich* [1982]. It would appear that the results of *Beuselinck et al.* [2002] for the individual size classes would have been better if they would have used larger settling velocities for the smallest size classes and smaller settling velocities for their largest size class, similar to the results obtained in this study (Table 2, Figure 5).

4.2. Possible Reasons for Different Settling Velocities

4.2.1. Flocculation

[40] It is likely that some of the particles moved down and off the flume in aggregates rather than as individual particles [*Alberts et al.*, 1980; *Slattery and Burt*, 1997]. These aggregates have a larger settling velocity than the individual particles. *Alberts et al.* [1980], for example, found that more than 80% of clay transported in rill and interrill erosion was transported in the aggregated form. This may be the case here for the clay, silt, and fine sand as well.

4.2.2. Selective Rainfall Detachment

[41] We assumed that rainfall detachment is nonselective with respect to size. Some studies have shown that splash is indeed a nonselective process [*Proffitt et al.*, 1993; *Mermut et al.*, 1997], while other studies have shown that splash is somewhat size selective [*Sutherland et al.*, 1996; *Wan and El-Swaify*, 1998; *Leguédois and Bissonnais*, 2004; *Asadi et al.*, 2007]. If rainfall detachment is size selective, then this would result in multiplication factors for the settling velocities (k_{vi}) that differ from unity.

4.2.3. Other Transport Mechanisms

[42] Some of the particles (especially the large particles) could have reached the overland flow collector by mechanisms other than those described by the Hairsine-Rose model (rainfall detachment and subsequent transport). The larger particles could, for example, have rolled over the surface or have moved by saltation, similar to bed load transport in rivers [*Bagnold*, 1973]. *Asadi et al.* [2007] also found that rolling or creeping or other mechanisms that are not well understood are operating and result in size selective particle movement. The underestimation of transport of coarse sediment in the multiclass net deposition model of *Beuselinck et al.* [2002] was also attributed to sediment rolling over the flume bed. These other transport mechanisms mainly influence the large sediment particles and could explain the observed maximum effective settling velocity of $\sim 3 \times 10^{-2}$ m/s for all particles >100 μm (Figure 5).

[43] Sediment splash could also result in an increased amount of large particles reaching the overland flow collector. The roof right above the overland flow collection trough minimized the amount of material that could splash directly into it. However, if the average splash distance was of the order of or larger than the distance a particle was transported before settling, this would increase the travel distance and result in smaller effective or optimized settling velocities for these particles. Bouncing of the particles when they hit the soil surface after falling back to the soil surface could also result in a larger residence time for the particles in the water and thus a smaller net settling velocity.

[44] The analytical equations were developed for rainfall driven soil erosion in the absence of flow-driven erosion. We thus assumed that rainfall-driven soil erosion was the dominant erosion mechanism. Flow-driven erosion [e.g., *Rose et al.*, 2007] will make some contribution at high slopes and high flow rates, but we can explain all of our observations ignoring the impact of this mechanism. All experiments could be modeled with the analytical equations for rainfall-induced soil erosion and all experiments could be represented with the same settling velocities. The relative errors for the high slope experiments were similar to the relative errors for the low slope experiments for which the adjusted settling velocities were determined (Table 3).

4.2.4. Shallow Water Depth

[45] The shallow water depths may have inhibited the particles from reaching their final settling velocities. The size of the largest particles ($\sim$1–2 mm) is of the same order of magnitude as the water depth (2–20 mm), and thus the large particles will be influenced by this most.

4.2.5. Hindered Settling

[46] The high sediment concentrations will likely result in hindered settling [*Richardson and Zaki*, 1954; *Batchelor*, 1972]. Particles bump into each other, slowing their settling velocity. In addition, the return flow of water around a particle creates an upward drag on neighboring particles, resulting also in a smaller net settling velocity. At the high sediment concentrations in this study the effect of hindered settling is likely important. *Baldock et al.* [2004], for example, showed that the hindered settling velocity reduces to less than half of the settling velocity in clear water at 15% of the maximum concentration. The effect of hindered settling is even larger for natural sand grains than for spheres [*Baldock et al.*, 2004; *Tomkins et al.*, 2005]. These effects would theoretically reduce the settling velocities of all particles.

4.2.6. Turbulence

[47] Some studies have found that net settling velocities are higher in homogeneous turbulent flows than in still water due to the preferential sweeping phenomenon as a result of the bias in particle inertia and therefore the nonrandom spatial distribution of particles in turbulent water [*Owen*, 1971; *Maxey*, 1987; *Wang and Maxey*, 1993; *Ruiz et al.*, 2004], while others have found that turbulence decreases the settling velocities [*Fung*, 1993]. Yet other studies have found that the settling velocities are reduced in weak turbulence and increased in strong turbulence and that at intermediate turbulence intensity heavy particles tend to be slowed while the settling velocity for small particles is increased [*Kawanisi and Shiozaki*, 2008]. It has also been shown that the velocity distribution of the settling particles can be significantly broadened and even be bimodal [*Pasquero et al.*, 2003].

[48] The exact influence of turbulence in the very shallow waters on the flume is not known. However, it is likely that

whether or not the average settling velocity is increased or decreased by turbulence, the residence time of some particles is increased because the actual settling velocity of individual particles can be very different from the average in turbulent flows. The transport distance of these particles is thus also increased compared with the average transport distance. This is especially important for the large particles that would otherwise settle almost instantaneously. The much slower settling smaller particles will be influenced mainly by a change in the average settling velocity.

4.2.7. Underestimation of the Infiltration Rate

[49] The vertical flow component due to the infiltrating water mainly influenced the very small particles because the settling velocity of these particles is smaller than or of the same order of magnitude as the infiltration rate (Figure 5a). While the steady overland flow rate was achieved quickly in the high-intensity experiments, the higher infiltration rates at the beginning of the experiments would result in a larger net settling velocity for the smallest size classes at the beginning of the experiments. Using too-low infiltration rates would result in multiplication coefficients for the settling velocities of the smallest size fractions that are larger than unity.

4.2.8. Measurement Errors

[50] Errors in the measurements of the settling velocities and errors in the measurement of the particle size distribution of the original soil would also result in multiplication coefficients for the settling velocities that differ from unity.

4.3. Parameter Definability

[51] All parameters except K were very well defined across a wide range of experimental conditions. We observed that aK was well defined for all size classes and that its optimum was similar for all size classes. The peak and steady state sediment concentrations are influenced by aK. A larger value for aK results in larger peak and steady state sediment concentrations. Both α and D are very well defined for the total concentration and the smallest particle size classes (<20 μm) but not for the larger particles. This is due mainly to the large scatter in the data and the more muted response for the large particles. The peak sediment concentration is controlled by α. The water depth (D) determines the decrease in sediment concentrations after the peak sediment concentration. Since only the total sediment concentration and the smallest size classes have a pronounced peak sediment concentration and subsequent decrease, it is logical that α and D are well defined for the smallest size classes and total concentration only. K influences the shape of the rising limb of the sediment graph (e.g., the time to peak sediment concentration). Since this period is very short for these high-intensity experiments and there are very few data points on this rising limb (two to three samples maximum but for many experiments only one sample, e.g., Figures 6–8), it is very difficult to determine the value of this parameter accurately. Hence K is not well defined for some of the experiments. However, K does not influence the modeled sediment concentrations very much because the time to peak sediment concentration is so short.

5. Conclusion

[52] Newly collected data from the 6-m × 2-m EPFL erosion flume were used to test the Hairsine-Rose model under more naturally realistic conditions than has been done so far. The analytical solutions from *Parlange et al.* [1999] were rewritten to account for infiltration. The analytical solutions could represent the total sediment concentrations well but could not represent the measured sediment concentrations of the individual size classes, especially the steady state concentrations and concentrations of the large particles, when the calculated or measured settling velocities were used. The individual size classes could be represented very well only when adjusted settling velocities were used. The smallest and midsize particles (<100 μm) settled faster than calculated or measured, while the largest particles (>315 μm) settled slower than measured. There was also a maximum settling velocity of $\sim 3 \times 10^{-2}$ m/s for all particles >100 μm. These adjusted settling velocities were found through manual optimization but could be calculated from the mass of material in the shield for each of the particle sizes at the end of the experiments as well. Once the settling velocities were optimized or calculated for one of the experiments, the analytical solutions of the Hairsine-Rose model could represent the data obtained under a wide range of moisture conditions and slopes. The parameters of the long-time solution (aK, α and D) were well defined over a wide range of conditions. The parameter for the short time solution (K) was not well defined for some of the experiments due mainly to the limited number of sediment samples collected during the short time to peak sediment concentration. In general, the model results were insensitive to the value of K.

References

Alberts, E. E., W. C. Moldenhauer, and F. R. Foster (1980), Soil aggregates and primary particles transported in rill and inter-rill flow, *Soil Sci. Soc. Am. J.*, *44*, 590–595.

Asadi, H., H. Ghadiri, C. W. Rose, and H. Rouhipour (2007), Interrill soil erosion processes and their interaction on low slopes, *Earth Surf. Processes Landforms*, *32*, 711–724, doi:10.1002/esp.1426.

Baba, J., and P. D. Komar (1981), Measurements and analysis of settling velocities of natural quartz sand grains, *J. Sediment. Petrol.*, *51*, 631–640.

Bagnold, R. A. (1973), The nature of saltation and of bed-load transport in water, *Proc. R. Soc. London A*, *332*, 473–504.

Baldock, T. E., M. R. Tomkins, P. Nielsen, and M. G. Hughes (2004), Settling velocity of sediments at high concentrations, *Coastal Eng.*, *51*, 91–100, doi:10.1016/j.coastaleng.2003.12.004.

Baril, P. (1991), Erodibilité des sols et érodabilité des terres: Application au plateau vaudois, Ph.D. thesis, 218 pp., Ecole Polytech. Féd. de Lausanne, Lausanne, Switzerland.

Basic, F., I. Kisic, O. Nestroy, M. Mesic, and A. Butorac (2002), Particle size distribution (texture) of eroded soil material, *J. Agron. Crop Sci.*, *188*, 311–322, doi:10.1046/j.1439-037X.2002.00567.x.

Batchelor, G. K. (1972), Sedimentation in a dilute dispersion of spheres, *J. Fluid Mech.*, *52*, 245–268, doi:10.1017/S0022112072001399.

Beuselinck, L., P. B. Hairsine, G. C. Sander, and G. Govers (2002), Evaluating a multiclass net deposition equation in overland flow conditions, *Water Resour. Res.*, *38*(7), 1109, doi:10.1029/2001WR000250.

Childs, E. C. (1969), *An Introduction to the Physical Basis of Soil Water Phenomena*, 493 pp., John Wiley, Hoboken, N.J.

Christiansen, J. E. (1942), *Irrigation by Sprinkling, Bull. 670*, Calif. Agric. Exp. Stn., Univ. of Calif., Berkeley.

Dietrich, W. E. (1982), Settling velocity of natural particles, *Water Resour. Res.*, *18*, 1615–1626, doi:10.1029/WR018i006p01615.

Ferguson, R. I., and M. Church (2004), A simple universal equation for grain settling velocity, *J. Sediment. Res.*, *74*, 933–937, doi:10.1306/051204740933.

Fung, J. C. H. (1993), Gravitational settling of particles and bubbles in homogeneous turbulence, *J. Geophys. Res.*, *98*(C11), 20,287–20,298, doi:10.1029/93JC01845.

Gabriels, D., and W. C. Moldenhauer (1978), Size distribution of eroded material from simulated rainfall: Effect over a range of texture, *Soil Sci. Soc. Am. J.*, *42*, 954–958.

Gao, B., M. T. Walter, T. S. Steenhuis, J.-Y. Parlange, K. Nakano, C. W. Rose, and W. L. Hogarth (2003), Investigating ponding depth and soil detachability for a mechanistic erosion model using a simple experiment, *J. Hydrol.*, *277*, 116–124, doi:10.1016/S0022-1694(03)00085-4.

Gibbs, R. J., M. D. Matthews, and D. A. Link (1971), The relationship between sphere size and settling velocity, *J. Sediment. Petrol.*, *41*, 7–18.

Hairsine, P. B., and C. W. Rose (1991), Rainfall detachment and deposition: Sediment transport in the absence of flow-driven processes, *Soil Sci. Soc. Am. J.*, *55*, 320–324.

Heilig, A., D. DeBruyn, M. T. Walter, C. W. Rose, J.-Y. Parlange, T. S. Steenhuis, G. C. Sander, P. B. Hairsine, W. L. Hogarth, and L. P. Walker (2001a), Testing a mechanistic soil erosion model with a simple experiment, *J. Hydrol.*, *244*, 9–16, doi:10.1016/S0022-1694(00)00400-5.

Heilig, A., D. DeBruyn, M. T. Walter, C. W. Rose, J.-Y. Parlange, T. S. Steenhuis, G. C. Sander, P. B. Hairsine, W. L. Hogarth, and L. P. Walker (2001b), Testing a mechanistic soil erosion model with a simple experiment, *J. Hydrol.*, *244*(1–2), 9–16, doi:10.1016/S0022-1694(00)00400-5. (Correction, *J. Hydrol., 317* (3–4), 171–172, 2006)

Jiménez, J. A., and O. S. Madsen (2003), A simple formula to estimate settling velocity of natural sediments, *J. Waterw. Port Coastal Ocean Eng.*, *129*, 70–78.

Kawanisi, K., and R. Shiozaki (2008), Turbulent effects on the settling velocity of suspended sediment, *J. Hydrol. Eng.*, *134*, 261–266, doi:10.1061/(ASCE)0733-9429(2008)134:2(261).

Leguédois, S., and Y. L. Bissonnais (2004), Size fractions resulting from an aggregate stability test, interrill detachment and transport, *Earth Surf. Processes Landforms*, *29*, 1117–1129, doi:10.1002/esp.1106.

Malam Issa, O., Y. L. Bissonnais, O. Planchon, D. Favis-Mortlock, N. Silvera, and J. Wainwright (2006), Soil detachment and transport on field- and laboratory-scale interrill areas: Erosion processes and the size-selectivity of eroded sediment, *Earth Surf. Processes Landforms*, *31*, 929–939, doi:10.1002/esp.1303.

Maxey, M. R. (1987), The gravitational settling of aerosol particles in homogeneous turbulence and random flow fields, *J. Fluid Mech.*, *174*, 441–465, doi:10.1017/S0022112087000193.

Mermut, A. R., S. H. Luk, M. J. M. Römkens, and J. W. A. Poesen (1997), Soil loss by splash and wash during rainfall from two loess soils, *Geoderma*, *75*, 203–214, doi:10.1016/S0016-7061(96)00091-2.

Miller, W. P., and M. K. Baharuddin (1987), Particle size of inter-rill-eroded sediments from highly weathered soils, *Soil Sci. Soc. Am. J.*, *51*, 1610–1615.

Mitchell, J. K., S. Mostaghimi, and M. Pound (1980), Primary particle and aggregate size distribution of eroded soil from sequenced rainfall events, *Trans. ASAE*, *26*, 1771–1777.

Owen, M. W. (1971), The effect of turbulence on the settling velocities of silt flocs, in *Proceedings of the 14th Congress of the International Association for Hydraulic Research*, vol. 4, pp. 27–32, Paris.

Parlange, J.-Y., W. L. Hogarth, C. W. Rose, G. C. Sander, P. Hairsine, and I. Lisle (1999), Addendum to unsteady soil erosion model, *J. Hydrol.*, *217*, 149–156, doi:10.1016/S0022-1694(99)00012-8.

Pasquero, C., A. Provenzale, and E. A. Spiegel (2003), Suspension and fall of heavy particles in random two-dimensional flow, *Phys. Rev. Lett.*, *91*, 054502, doi:10.1103/PhysRevLett.91.054502.

Proffitt, A. P. B., C. W. Rose, and P. B. Hairsine (1991), Rainfall detachment and deposition: Experiments with low slopes and significant water depths, *Soil Sci. Soc. Am. J.*, *55*, 325–332.

Proffitt, A. P. B., C. W. Rose, and C. J. Lovell (1993), Settling velocity characteristics of sediment detached from a soil surface by raindrop impact, *Catena*, *20*, 27–40, doi:10.1016/0341-8162(93)90027-M.

Richardson, J. F., and W. N. Zaki (1954), Sedimentation and fluidization: 1, *Trans. Inst. Chem. Eng.*, *32*, 35–53.

Rose, C. W., W. L. Hogarth, G. Sander, I. Lisle, P. Hairsine, and J.-Y. Parlange (1994), Modeling processes of soil erosion by water, *Trends Hydrol.*, *1*, 443–451.

Rose, C. W., B. Yu, H. Ghadiri, H. Asadi, J.-Y. Parlange, W. L. Hogarth, and J. Hussein (2007), Dynamic erosion of soil in steady sheet flow, *J. Hydrol.*, *333*, 449–458, doi:10.1016/j.jhydrol.2006.09.016.

Ruiz, J., D. Macias, and F. Peters (2004), Turbulence increases the average settling velocity of phytoplankton cells, *Proc. Natl. Acad. Sci. U.S.A.*, *101*, 17,720–17,724, doi:10.1073/pnas.0401539101.

Sander, G. C., P. B. Hairsine, C. W. Rose, D. Cassidy, J.-Y. Parlange, W. L. Hogarth, and I. G. Lisle (1996), Unsteady soil erosion model, analytical solutions and comparison with experimental results, *J. Hydrol.*, *178*, 351–367, doi:10.1016/0022-1694(95)02810-2.

Slattery, M. C., and T. P. Burt (1997), Particle size characteristics of suspended sediment in hillslope runoff and stream flow, *Earth Surf. Processes Landforms*, *22*, 705–719, doi:10.1002/(SICI)1096-9837(199708)22:8<705::AID-ESP739>3.0.CO;2-6.

Stokes, G. G. (1851), On the effect of the internal friction on the motion of pendulums, *Cambridge Philos. Trans., Part 2*, *2*, 8–106.

Sutherland, R. A., Y. Wan, A. D. Ziegler, C.-T. Lee, and S. A. El-Swaify (1996), Splash and wash dynamics: An experimental investigation using an oxisol, *Geoderma*, *69*, 85–103, doi:10.1016/0016-7061(95)00053-4.

Swanson, N. P., A. R. Dedrick, and H. E. Weakly (1965), Soil particles and aggregates transported in runoff from simulated rainfall, *Trans. ASAE*, *8*, 437–440.

Tomkins, M. R., T. E. Baldock, and P. Nielsen (2005), Hindered settling of sand grains, *Sedimentology*, *52*, 1425–1432.

Viani, J.-P. (1986), Contribution à l'étude expérimentale de l'érosion hydrique, Ph.D. thesis, 239 pp., Ecole Polytech. Féd. de Lausanne, Lausanne, Switzerland.

Wan, Y., and S. A. El-Swaify (1998), Characterizing interrill sediment size by partitioning splash and wash processes, *Soil Sci. Soc. Am. J.*, *62*, 430–437.

Wang, L.-P., and M. R. Maxey (1993), Settling velocity and concentration distribution of heavy particles in homogeneous isotropic turbulence, *J. Fluid Mech.*, *256*, 27–68, doi:10.1017/S0022112093002708.

Young, R. A., and C. A. Onstad (1976), Predicting particle-size composition of eroded soil, *Trans. ASAE*, *19*, 1071–1075.

D. A. Barry, M. B. Parlange, and M. F. Tromp, Institute of Environmental Science and Technology, School of Architecture, Civil and Environmental Engineering, Ecole Polytechnique Fédérale de Lausanne, CH-1015 Lausanne, Switzerland. (andrew.barry@epfl.ch; marc.parlange@epfl.ch; martin_tromp@hotmail.com)

J.-Y. Parlange and M. T. Walter, Department of Biological and Environmental Engineering, Cornell University, Ithaca, NY 14853-5701, USA. (jp58@cornell.edu; mtw5@cornell.edu)

G. C. Sander, Department of Civil and Building Engineering, Loughborough University, Loughborough LE11 3TU, UK. (g.sander@lboro.ac.uk)

H. J. Tromp-van Meerveld, Department of Geography, Simon Fraser University, 8888 University Drive, Burnaby, British Columbia, Canada V5A-1S6. (ilja@sfu.ca)